Available online at www.sciencedirect.com
ScienceDirect
Acta Materialia 56 (2008) 1813–1819
Acta MATERIALIA
www.elsevier.com/locate/actamat

Strengthening gold thin films with zirconia nanoparticles for MEMS electrical contacts

Jesse R. Williams, David R. Clarke *

Materials Department, College of Engineering, University of California, Santa Barbara, CA 93106-5050, USA

Received 19 July 2007; received in revised form 10 December 2007; accepted 16 December 2007
Available online 21 February 2008

Abstract

Thin gold films can be strengthened by the incorporation, during reactive sputtering, of nanosized dispersions of monoclinic zirconia. Micron-thick films containing ~2 vol.% zirconia particles having a particle size of 1–3 nm are found to have an indentation hardness of 3.8 GPa after annealing for 60 h at 500 °C in air. Sputtered gold films of the same thickness and annealed under the same conditions had a hardness of 2.3 GPa. The nanoparticles of zirconia resist coarsening with no change in diameter between deposition and after 60 h at 500 °C. They also suppress grain growth of the gold grains. The electrical resistivity of the strengthened gold films was 4.5 μΩ cm, about 55% higher than gold films. The temperature coefficient of resistivity was unaffected.

Keywords: Gold; MEMS; Sputter deposition; Indentation

1. Introduction

The development of resistive electrical contacts in microelectromechanical systems (MEMS) devices [1] poses several additional constraints over and above the usual requirements for bulk electrical contacts and switches [2]. For instance, apart from the contacts being smaller in size, the forces available for making and breaking contact are significantly smaller. Consequently, the contacts are more susceptible to stiction even in the absence of welding since the forces to pull them apart are limited. The smaller forces available for bringing the contacts together also mean that it is less likely to be possible to break through any superficial oxide to make electrical contact. In addition, the smaller size implies that surface roughness may play a more important role than in bulk contacts. In fact, the majority of MEMS electrical contacts appear to operate under conditions where adhesive contact mechanics are the appropriate mechanics [3]. Hence, the surface energies, surface roughness, geometry, elastic constants and plastic deformation all influence the behavior of the contacts [4–6].

Aside from the mechanics of contacts, MEMS contacts must have, like their bulk counterparts, low electrical conductivity and be stable both to Joule heating and electromigration while carrying current. This, in turn, means that the mechanical properties should be relatively insensitive to temperature even though the spark erosion resulting from electrical discharge can, with appropriate electrical design, be avoided so that currents only flow once electrical contact is made. Furthermore, in contrast to many bulk electrical switches, electrical switches in MEMS devices, especially for radiofrequency applications [1], must be capable of sustaining millions to billions of switching cycles.

Ideally, apart from initial local flattening of some asperities associated with any initial mechanical shakedown, electrical contacts should remain elastic over their life. This requires that the contact material has a high yield stress at ambient as well as at high temperature and a high creep resistance. These properties are required not just to prevent welding by plastic flow, but also stiction [5].

* Corresponding author. Tel.: +1 805 893 8275.
E-mail address: clarke@engineering.ucsb.edu (D.R. Clarke).

1359-6454/$34.00
doi:10.1016/j.actamat.2007.12.038

A variety of metals have been used in bulk electrical contacts, but gold has traditionally been the metal of choice for high-performance electrical contacts and switches on account of its chemical inertness, and relatively low electrical resistance [2]. In those cases requiring a harder contact material, gold is strengthened by solid solution alloying, with metals such as nickel, copper, silver, platinum or palladium. Even though the use of nickel and copper alloying promotes the formation of a superficial oxide that increases the contact electrical resistance, they are acceptable in many bulk applications because the switch forces are designed to be sufficiently large to break through the oxides. In addition, although, solid solution hardening has the advantage of scaling down to the dimensions of MEMS contacts, solid solution hardening is not very effective at high temperatures. Any alternative strengthening mechanism must also operate on a small scale, much smaller than the contact area, so that the deformation is uniform over the contact.

In this work, we describe the strengthening of gold films by incorporating nanoparticles of zirconium dioxide (zirconia) during film deposition. This dispersion hardening approach is expected to provide hardening to higher temperatures than either solution or precipitation hardening. The zirconia–gold system was selected for several reasons. Zirconium has only limited solubility in gold and its oxide has a large heat of formation. Consequently, there is an expectation that sputtered zirconium ions in the plasma would react with oxygen ions to form zirconia particles during deposition. In addition, it might also be expected that the large heat of formation would result in a very small particle size since the zirconium ions would effectively getter oxygen ions in their immediate vicinity. Once formed, the zirconium dioxide particles would be expected to be stable against coarsening on account of the limited solubility of both zirconium and oxygen in gold. Furthermore, and relatedly, being oxide dispersion with a very high melting temperature, the particles are stable at high temperatures and can be expected to confer creep resistance to the gold films.

2. Experimental

Films with thicknesses of greater than 1 μm were prepared by sputtering onto silicon wafers having a thick (500 nm) thermal oxide. The thick thermal oxide was used to prevent diffusion between the gold films and the silicon during subsequent heat treatments. Gold films with nanodispersed zirconia were sputtered from an alloyed Au–2 at.% Zr metal target in a stable argon–oxygen (Ar–O) plasma. The plasma was maintained at a pressure of 12 mTorr with gas flows of 40 and 1 sccm of Ar and O, respectively, and at a constant power of 200 W. The corresponding voltage and current were approximately 490 V and 400 mA, with the actual values being determined by the control system of the sputtering system to maintain constant power. Prior to the reactive sputtering of the gold–zirconia films, a thin adhesion layer of titanium was first deposited in an Ar-plasma followed by about 30 nm of the gold–zirconia film, again deposited in an Ar-plasma. Once these thin layers were deposited, the gas was switched to an Ar–O mixture for the reactive ion sputtering of the gold–zirconia. The thin gold–zirconia metal layer was found to be necessary to improve adhesion, otherwise the titanium adhesion layer was found to be ineffective. Presumably, the gold–zirconia layer prevented oxidation of the titanium in the Ar–O plasma used for the subsequent reactive ion sputtering. All three layers were sputtered sequentially without breaking vacuum. For comparison purposes, pure gold films with thicknesses between 1 micron and 5 μm were deposited under similar conditions but in a pure Ar atmosphere. A titanium adhesion layer was deposited prior to depositing the pure gold films again without breaking vacuum.

Some films were subsequently annealed in a rapid thermal annealing system in a N_2 atmosphere for different times and temperatures, up to 500 °C for 10 min. Others were annealed in air for up to 60 h at 500 °C.

The microstructure of the films was examined by transmission electron microscopy (TEM) at 300 kV of thin foils prepared by ion milling. The final stage of the ion milling was carried out at low voltage and current to minimize ion-induced damage. This was of particular concern as high-energy ion milling can produce 5–10 nm voids. Atomic force microscopy (AFM) was used to measure the grain size, and to determine the average surface roughness (R_a). R_a was calculated from 5×5 μm image scans of the surface, each image consisting of 1024×1024 data points.

Hardness measurements were made using a Hysitron Triboscan nanoindenter fitted with a cube-corner diamond indenter. Indents were applied with monotonic loading (as opposed to the continuous stiffness method). Individual indents were performed using peak loads ranging from 100 to 2000 μN so as to provide information on any depth-dependent hardness. The highest loads corresponded to a maximum depth of 200 nm depth. All the films indented were greater than 1 μm thick. Indentation using a cube-corner rather than the more common Berkovich indenter was chosen for two principal reasons. Firstly, initial experiments suggested that there was greater scatter in the Berkovich data which was attributed to its greater sensitivity to surface roughness. Secondly, the cube-corner indenter produces greater plastic strain for the same depth of indentation than the Berkovitch and so is more effective in producing deformation in films of limited thickness. Typical micrographs of the cube-corner indentations used to determine hardness are shown in Fig. 1.

The electrical resistance of the films was made from serpentine conduction lines fashioned from blanket films using standard photolithography and lift-off processing. The lines were 1 μm thick, 30 μm wide and 2 m long. A four-point probe configuration was used to increase electrical sensitivity and current–voltage (I/V) characteristics were measured using a HP 4156 semiconductor parametric

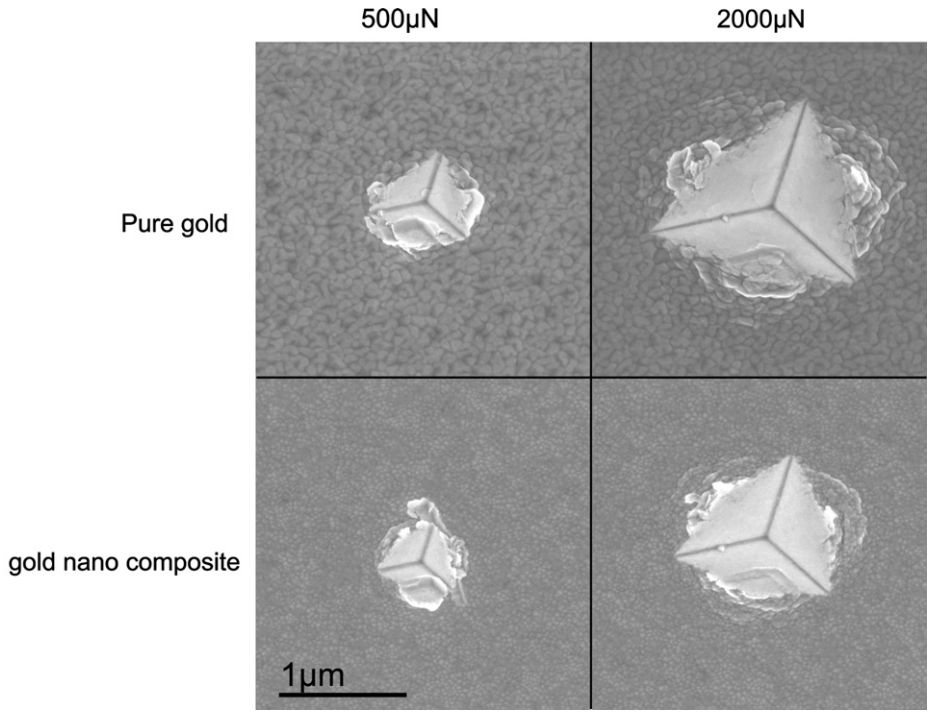

Fig. 1. Illustration of the cube-corner indentations into the pure and zirconia-containing gold films at two different loads. The coarser grain structure of the pure gold films is evident. Scanning electron micrographs.

analyzer. The temperature dependence of the resistance of the lines was determined by first heating the samples to 100 °C and the resistance measured upon cooling with a thermocouple attached to the film surface. The resistivity was also measured before and after annealing.

3. Results

In their as-deposited state, all the nano-zirconia gold and the pure gold films had a columnar microstructure with grains oriented in the growth direction and with a ⟨1 1 1⟩ texture. This is characteristic of sputter-deposited gold films [7,8]. Both types of films exhibited a high degree of twinning. The twin spacing was 4.3 ± 0.4 nm for the nano-gold samples and 5.4 ± 0.6 nm for the pure gold samples. The major difference between the films was that the lateral grain size of the columns, measured parallel to the plane of the films, of the zirconia-containing films was somewhat smaller, 50 nm in diameter, compared to pure gold, 100 nm in diameter (Fig. 2).

Selected-area diffraction (SAD) patterns (Fig. 3) confirmed the presence of zirconia in the films. Detailed analysis of the ring patterns indicated that the zirconia was monoclinic rather than either cubic or tetragonal. The defining features were the reflections at large interplanar spacings not present in diffraction pattern of tetragonal

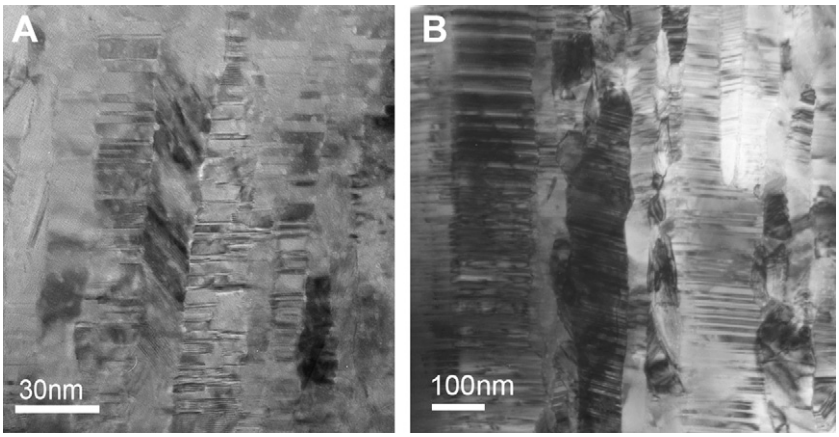

Fig. 2. TEM cross sections of the as-sputtered microstructure of the zirconia-containing gold (A) and pure gold films (B).

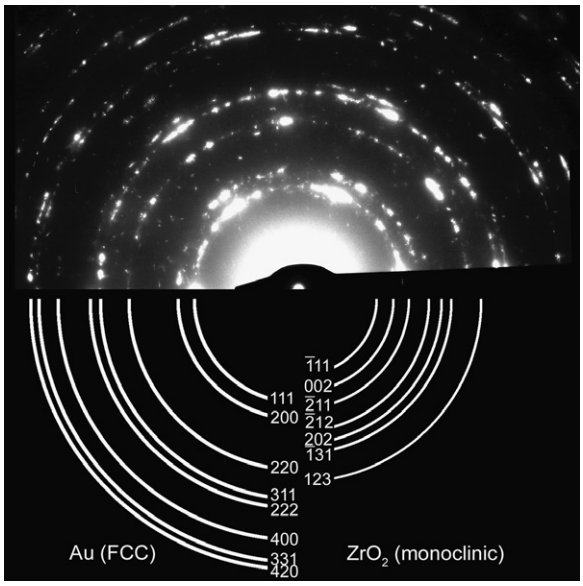

Fig. 3. Selected-area diffraction pattern recorded from the gold film containing zirconia. The diffractions rings corresponding to gold and monoclinic zirconia are labeled.

zirconia [9]. The diffraction spots in the zirconia rings were very faint, presumably because of their low volume fraction and the low electron scattering coefficient of zirconia relative to that of gold. Although, it was difficult to distinguish the nanoparticles under standard imaging conditions, they were evident under Fresnel contrast imaging (Fig. 4). In this method, over- or under-focusing produces Fresnel contrast at the interface between the two phases. This technique was first used to characterize thin interfacial films [10]. By using this imaging technique the particles are found to have diameters of 1–3 nm. The volume fraction of particles was estimated to be 0.025 ± 0.01 based on the projected number of particles and the estimated film thickness. The lower value of the volume fraction is consistent with assuming that some of the zirconium in the target was lost during sputtering and the higher value is consistent with assuming that all the zirconium in the target (2 at.% Zr) is transferred to the film and converted to zirconium dioxide. It is likely that the actual value is between these two values.

The microstructural evolution of the two materials upon annealing was very different. Extensive grain growth occurred in the pure gold films. Ten minutes at 300 °C produced equiaxed grains, hundreds of nanometers in size. Concurrently, the number of twins reduced considerably. Ten minutes annealing at 400 °C resulted in through-film grain growth, and lateral growth of grains to over a micron in size. The reactively sputtered gold–zirconia material, however, exhibited negligible grain growth through temperatures to 500 °C. Even when the material was annealed for 60 h at 500 °C, the lateral grain size remained below 100 nm (Fig. 5). The size of the zirconia particles was not affected by heat treatment, and even after annealing at 500 °C they were still in the range of 1–3 nm. AFM images of the gold–zirconia material after annealing at 500 °C indicate that the surface roughness (R_a) was 1.26 nm which compared with the surface roughness of the annealed gold films of 2.33 nm (Table 1).

The nanoindentation results clearly showed that the gold–zirconia films were substantially harder than the pure gold films (Fig. 6). Each data point corresponds to a differ-

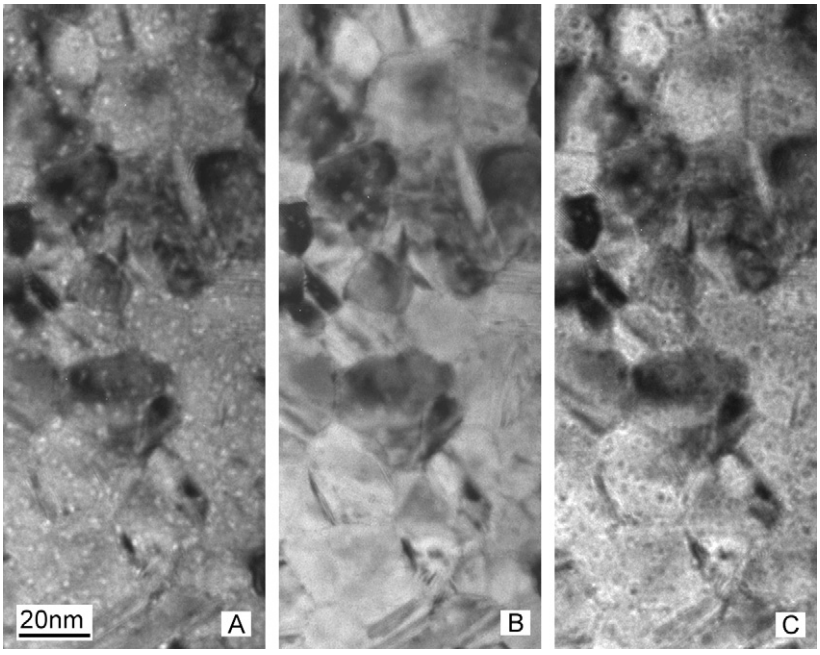

Fig. 4. Through-focus series of a gold film containing zirconia particles after annealing at 500 °C for 60 h to enhance the visualization of the zirconia particles. A is under-focused, B is in focus, and C is over-focused.

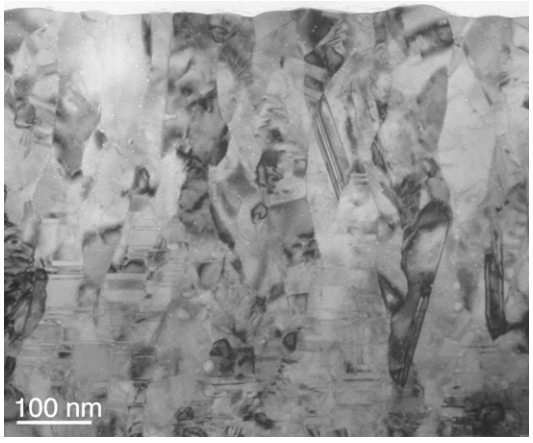

Fig. 5. TEM cross-section of the same film as in Fig. 3. Although the point defects and many of the twin boundaries are annealed out, the lateral grain size remains around 50 nm.

Table 1
Summary of measured physical properties

	Lateral grain size	Hardness (GPa)	Resistivity (μΩ cm)	Roughness (nm)
Gold–zirconia as-sputtered	50 nm	5.0	6.2	1.15
Gold–zirconia annealed 500 °C	50 nm	3.8	4.5	1.26
Pure gold as-sputtered	100 nm	2.7	4.0	2.11
Pure gold annealed 500 °C	~1 μm	2.3	3.4	2.33

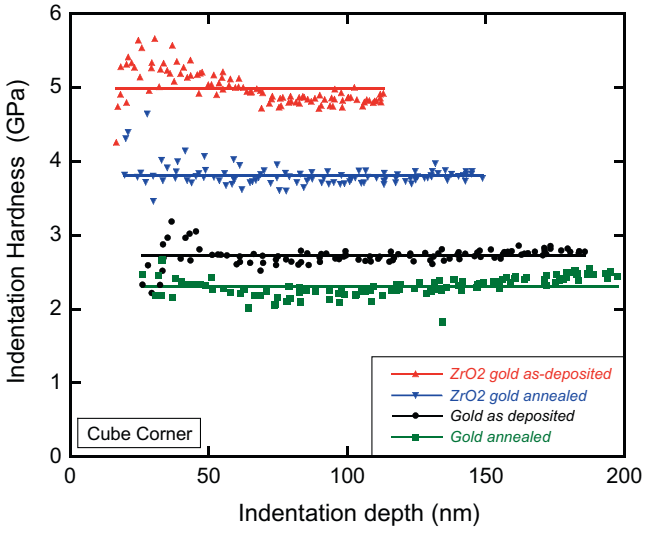

Fig. 6. Cube-corner indentation hardness of the as-deposited films and after annealing for 10 min at 500 °C. Each data point corresponds to a different indentation. The lines are least-square fits to the data and indicate a lack of any size-dependent hardness.

ent indentation. In their as-deposited conditions, the gold–zirconia films and pure gold films had hardnesses of 5.0 and 2.7 GPa, respectively. (The hardness of the pure gold films is higher than that cited in the literature [11–13], but this is

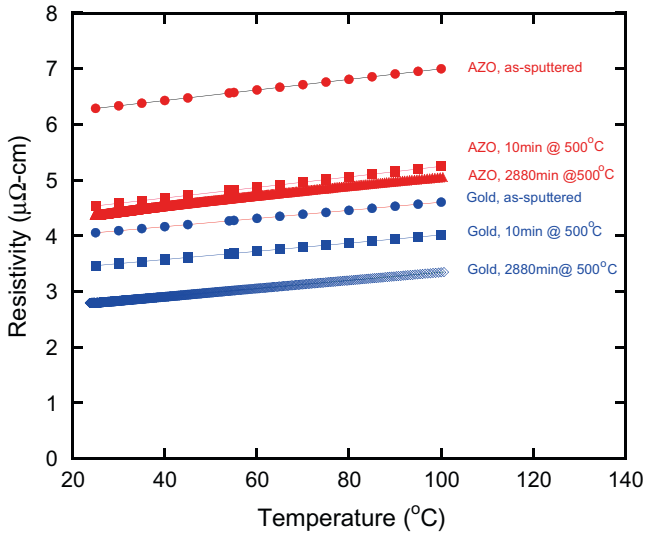

Fig. 7. Electrical resistivity of the sputtered gold films and the zirconia-containing gold (AZO) films in their as-deposited state and after the annealing treatments indicated.

attributed to using a cube-corner rather than a Berkovitch indenter tip). After annealing at 500 °C for 10 min, the hardness of the two materials dropped to 3.8 and 2.3 GPa, respectively. No distinct size effect on hardness was noted.

The resistivity results, and their temperature dependence, are shown in Fig. 7 and listed in Table 1. The resistivity of the as-deposited zirconia-strengthened gold and the pure gold films were measured to be 6.2 and 4.0 μΩ cm, respectively. After annealing at 500 °C for 10 min these resistivities dropped to 4.5 and 3.4 μΩ cm.

4. Discussion

Dispersing nanoparticles of zirconia during deposition has proven to be an effective means of increasing the hardness of thin gold films. Although the initial, exceptional hardness (5 GPa) after deposition decreases upon annealing, it remains almost twice that of pure gold deposited under the same conditions and subject to the same annealing conditions. The initial drop in hardness of both the zirconia-dispersed gold and pure gold is attributed to annealing out of point defects, and additionally, in the case of pure gold, to grain coarsening. The other key observations are that the zirconia particles also have the effect of stabilizing the grain structure of the gold film and the zirconia particles themselves appear resistant to coarsening. Although we were unable to resolve the interface between the zirconia particles and the gold by TEM, we assume that the zirconia particles are incoherent.

Before discussing the hardness values of the zirconia-containing films, it is appropriate to comment on the higher hardness of the sputtered gold films we measure compared to that in the literature. As remarked earlier we attribute this to using a cube-corner indenter, which

has a different tip geometry than the Berkovich tip used in the reported studies. The cube-corner tip is much sharper (a semi-angle of 35.26°) than the Berkovich tip. This makes it less susceptible to surface roughness variations from place to place and the representative plastic strain produced is also larger. For an indentation tip of self-similar geometry, this can be approximated from the angle β, the complement of the tip semi-angle; as follows:

$$\epsilon_R \approx 0.2 \tan \beta. \tag{1}$$

Using a conical approximation of the pyramidal tip, this angle is 19.7° for a Berkovich tip and 47.7° for the cube-corner tip [14]. Substituting in Eq. (1), the representative strain produced by the Berkovich tip and cube-corner tip are 7% and 22%, respectively, suggesting that the higher hardness we measure is associated with the larger plastic strain, presumably because of a greater propensity to work hardening. (It is recalled that Tabor's insight was that the hardness was equal to three times the yield stress at 0.08 strains [15] and that the hardness generally scales with work hardening [16].) In the absence of any contrary information, we assume in the following that the yield stress is one-third of the hardness measured by the cube-corner technique.

In discussing the measured hardness values, we start with the hardness of the annealed, pure gold films. As is well established, the hardness of gold films is substantially greater than that of the bulk, irrespective of the method used to measure the hardness. This is attributed to the difficulty in moving dislocations in thin films [17,18]. In the following we take the hardness of the annealed gold, which has a grain size of ~1 μm, to represent the base level in discussing the hardness of the other gold films. The greater hardness of the as-deposited gold film is consistent with the increase in yield stress associated with the smaller grain size of 100 nm determined from TEM. Using the Hall–Petch relation

$$\Delta\sigma_{\mathrm{HP}} = Kd^{-0.5}, \tag{2}$$

where K is a constant and d is the lateral grain size, the increase in yield stress is 0.20 GPa. (For face-centered cubic metals, K is approximately equal to: $\mu b^{1/2}/15$, where μ and b are the shear modulus and Burgers vector. For gold, they are 27 GPa and 0.288 nm, respectively, so K has a value of ~0.966 GPa$\sqrt{\mathrm{nm}}$). Assuming that the hardness is three times the yield stress [15], and then the hardness is 0.6 GPa higher than that of the annealed gold. This is somewhat greater than that measured, namely 0.4 GPa, as shown in Fig. 6.

The presence of zirconia nanoparticles and the smaller lateral grain size distinguish the annealed gold films containing zirconia nanoparticles, suggesting that the greater hardness can be attributed to a combination of dispersion hardening and the smaller grain size. The grain size contribution, $\Delta\sigma_{\mathrm{HP}}$, can be calculated using the Hall–Petch equation with the same coefficients as above. For the grain size of the zirconia-containing gold film (~50 nm), the grain size contribution to the yield stress is estimated from Eq. (1) to be 0.41 GPa. The contribution to the yield stress of dispersion hardening, $\Delta\sigma_{\mathrm{D}}$, can be estimated from particle size and volume fraction using the Orowan equation and assuming that dislocations cannot cut through the particles [19]

$$\Delta\sigma_{\mathrm{D}} = \alpha\frac{\mu b}{L} = \alpha\frac{2\mu b}{d}\sqrt{\frac{f}{\pi}}, \tag{3}$$

where L is the interparticle spacing, d is the nanoparticle diameter and f is the volume fraction of particles. α is a numerical constant, believed to be about unity. Taking the volume fraction of zirconia particles as 0.025 ± 0.010 and the average particle diameter of 2 ± 1 nm, the dispersion hardening contribution is estimated to be ~0.69 GPa. The estimate is particularly sensitive to the nanoparticle diameter which, unfortunately, is the least well characterized parameter in our studies.

As in other areas of dislocation plasticity, the question arises how to appropriately combine the contributions to the yield stress from a number of mechanisms. One method is to simply add the individual contributions, which generally overestimates the yield stress. If it can be assumed that the yield stress contributions can simply be added, then the hardness contributions can also be added. Adding the increases in yield stress due to the smaller grain size and dispersion hardening to the base film yield stress, and multiplying by three gives a total hardness of 5.6 GPa. The other method is to add the contributions to the overall yield stress in quadrature so that the effective yield stress is given by

$$\Delta\sigma_Y = \sqrt{(\Delta\sigma_{\mathrm{HP}})^2 + (\Delta\sigma_{\mathrm{D}})^2}. \tag{4}$$

Making the argument that the increase in hardness over that of the base gold can be calculated by adding the yield stress of the base gold film in quadrature to the grain size contribution and dispersion hardening, the total yield stress of the nanoparticle-strengthened gold would be 1.13 GPa, corresponding to an overall, total hardness of 3.4 GPa. Although the latter is somewhat lower than the value of 3.8 GPa measured, it is well within the limits associated with the uncertainty in particle diameter and volume fraction.

The electrical resistivity of the zirconia-strengthened gold films is, as expected, larger than that of the sputtered pure gold films from room temperature up to 500 °C, even though both sets of films exhibit a reduced resistivity after annealing at 500 °C as indicated in Fig. 7. The resistivity of the pure gold films decreases significantly with annealing from 4.0 μΩ cm in its as-deposited condition to 3.4 μΩ cm after 10 min to 2.8 μΩ cm after 48 h at 500 °C. This decrease is attributed to the reduction in the number of point defects formed during sputtering and possibly the reduction in twin density together with the concurrent increase in grain size. After annealing, the value is larger than the literature value for bulk gold, 2.3 μΩ cm [2]. This is attributed to scattering from both the grain boundaries

[20] and from roughness of the sides and surfaces of the serpentine lines [21]. Although the thickness of the films, ~1 μm, is larger than the estimated electron mean free path (~40 nm at room temperature [22]) and larger than the size considered in models for size effects [23–25], the small lateral grain size leads to a large number of grain boundaries per unit length. Furthermore, the ratio of interfacial area to volume in the serpentine lines is very high, $\sim 2 \times 106\ m^{-1}$, which suggests a sensitivity to the surface roughness of the lines. The resistivity of the gold films containing zirconia nanoparticles exhibits a similar proportional drop upon annealing as do the pure gold films. As the grain size remains unchanged, the drop is attributed to annealing out of some of the point defects, and possibly some additional formation of zirconia from O and Zr in solid solution. However, the fact that the resistivity does not significantly decrease after 10 min annealing at 500 °C suggests that the resistivity is dominated by the remaining grain boundaries, scattering from the nanoparticles and, possibly, Zr and Ar atoms in solid solution. As the solubility of oxygen in gold is low (less than 10^{-7} moles O_2 per mole of gold at 300 K [26]) there is also little likelihood of any excess Zr atoms reacting with oxygen from the atmosphere to form zirconia, even at 500 °C, to further decrease impurity scattering. (It is pertinent to add that high-temperature annealing, typically at ~900 °C, in an oxidizing atmosphere is a proven means of lowering the resistivity of noble metals containing oxidizable impurities [27,28].) We are left to conclude that the higher resistivity is due to electron scattering from a combination of excess Zr and Ar in solid solution as well as the small interparticle spacing of the monoclinic zirconia nanoparticles.

The reactive sputtering route to producing nanoparticle-strengthened films has several advantages over other methods, such as internal oxidation of a gold alloy and ion implantation. Arbitrarily thick films can be produced as the thickness of the oxide formation is not dependent on either the diffusion of oxygen, as it is in internal oxidation, or on the implantation range. In addition, the oxide dispersion is produced during deposition, whereas internal oxidation requires prolonged heating at high temperatures to facilitate inward diffusion of oxygen, a process incompatible with MEMS processing. The same conclusions would pertain for the formation of nitrides or carbides by internal nitridation or carburization.

Finally, it is emphasized that although impressive increases in hardness have been achieved, the processing of our zirconia nanoparticle-strengthened gold films has not been optimized. It is likely that further enhancements in hardness as well as in maximizing hardness while minimizing electrical resistance can be achieved by more systematic investigation of the reactive sputtering conditions and their correlation to the zirconia particle size and distribution.

5. Conclusions

Gold films containing dispersions of monoclinic zirconia particles, 1–3 nm in diameter, have been produced by reactive ion sputtering in an Ar–O atmosphere. The films are 1.8 times harder than pure gold film deposited under similar conditions, even after annealing at 500 °C. The increase in hardness is attributed primarily to the dispersion of zirconia nanoparticles. The zirconia nanoparticles are also effective in limiting grain growth even up to 500 °C for 60 h. The resistivity of the gold films containing the zirconia nanoparticles were 1.3 times higher than that of the annealed pure gold films.

Acknowledgments

This work was supported by the US Army Space and Missile Defense Command through DARPA grant W9113-04-01-0001. The content does not necessarily reflect the position or policy of the Federal Government.

References

[1] Rebeiz GM, Mems RF. Theory, design and technology. Hoboken, NJ: Wiley; 2003.
[2] Holm R. Electric contacts: theory and applications. 4th ed. Berlin: Springer; 2000.
[3] Johnson KL. Contact mechanics. New York: Cambridge University Press; 1985.
[4] Pashley MD, Pethica JB. J Vac Sci Technol 1985;3:757.
[5] Gregori G, Clarke DR. J App Phys 2006;100:094904.
[6] Johnson LL, Kendall K, Roberts AD. Proc Roy Soc Lond A 1971;324:301.
[7] Pashley DW. Adv Phys 1956;5:173.
[8] Rudiger O. Ann Phys 1937;30:505.
[9] JCPDF, Files 88-1007 and 83-0944.
[10] Clarke DR. Ultramicro 1979;4:33.
[11] Lilleodden ET, Nix WD. Acta Mater 2006;54:1583.
[12] Pruitt BL, Kenny TW. Sensor Actuator A 2003;104:68.
[13] Tayebi N, Polycarpou AA, Conry TF. J Mater Res 2004;19:1791.
[14] Fischer-Cripps AC. Nanoindentation. New York: Springer; 2002.
[15] Tabor D. The hardness of metals. Oxford: Claredon Press; 2000.
[16] Bowden FP, Tabor D. The friction and lubrication of solids. London: Oxford University Press; 1954.
[17] Nix WD. Met Trans A 1989;20:2217.
[18] Freund LB, Suresh S. Thin film materials. Cambridge: Cambridge University Press; 2003.
[19] Brown LM, Ham RK. Dislocation–particle interactions. In: Kelly A, Nicholson RB, editors. Strengthening methods in crystals. Amsterdam: Elsevier; 1971. p. 12.
[20] Mayadas AF, Shatzkes M. Phys Rev B 1970;1:1382.
[21] Rossnagel SM, Kuan TS. J Vac Sci Techol B 2004;22:240.
[22] Ashcroft NW, Mermin ND. Solid state physics. New York: Holt, Rinehart and Winston; 1976.
[23] Sondheimer EH. Adv Phys 1952;1:1.
[24] Fuchs K. Cambridge Philos Soc 1938;34:100.
[25] Steinhogel W et al. Phys Rev B 2002;46:075414.
[26] Eichenauer W, Muller G. Zeit Metallkunde 1962;53:321.
[27] Svoboda P. J Phys F: Met Phys 1978;8:1757.
[28] Ehrlich AC. J Mater Sci 1974;9:1064.